Evaluation of model complexity and space-time resolution on the prediction of long-term soil salinity dynamics

G. Schoups, J.W. Hopmans*, and K.K. Tanji

Hydrology Program, Department of Land, Air and Water Resources (LAWR), University of California, Davis, CA 95616, USA;

*Corresponding author: jwhopmans@ucdavis.edu; Phone 530-752-3060; Fax 530-752-5262

Abbreviations: TDS, total dissolved solids; SAR, sodium adsorption ratio; CEC, cation exchange capacity; R, reactions; NR, no reactions; CPU, central processing unit.

Evaluation of model complexity and space-time resolution on the prediction of long-term soil salinity dynamics

ABSTRACT

The numerical simulation of long-term large-scale (field to regional) variably-saturated subsurface flow and transport remains a computational challenge, even with today's computing power. Therefore, it is appropriate to develop simplified models that focus on the main processes operating at the pertinent time and space scales, as long as the error introduced by the simpler model is acceptable compared to the uncertainties associated with the spatial and temporal variation of boundary conditions and parameter values. This study investigates the effects of various model simplifications on the prediction of long-term soil salinity and salt transport in irrigated soils. Average root-zone salinity and cumulative annual drainage salt load were predicted for a 10-year period using a one-dimensional numerical flow and transport model (UNSATCHEM) that accounts for solute advection, dispersion and diffusion, and complex salt chemistry. The model uses daily values for rainfall, irrigation, and potential evapotranspiration rates that are representative for the western San Joaquin Valley, CA. Model simulations consist of benchmark scenarios with a fine spatial resolution for different hypothetical cases that include shallow and deep water table, different leaching fractions and soil gypsum content, and shallow groundwater salinity, with and without soil chemical reactions. These hypothetical benchmark simulations are compared with the results of various model simplifications that considered

(i) annual average boundary conditions, (ii) coarser spatial discretization, and (iii) reducing the complexity of the salt-soil reaction system. Based on the 10-year simulation results, we conclude that salt transport modeling does not require daily boundary conditions, a fine spatial resolution, or complex salt chemistry. Instead, if the focus is on long-term salinity, a simplified modeling approach can be used, using annually-averaged boundary conditions, a coarse spatial discretization, and inclusion of soil chemistry that only accounts for cation exchange and gypsum dissolution-precipitation. We also demonstrate that prediction errors due to these model simplifications may be small, when compared to effects of parameter uncertainty on model predictions. The proposed model simplifications lead to larger time steps and reduced computer simulations times by a factor of 1,000.

Key words Soil salinity, gypsum, unsaturated flow, multi-component transport, major ion chemistry

INTRODUCTION

The numerical simulation of long-term large-scale (field to regional) variably-saturated subsurface flow and transport remains a computational challenge, even with today's computing power. Therefore, it is appropriate to develop and use simplified models that focus on the main processes operating at the pertinent time and space scales, as long as the error introduced by the simpler model is acceptably small compared to the uncertainties associated with the spatial and temporal variation of boundary conditions and parameter

values. A key question, however, is related to the upscaling of point-scale physical and chemical processes to the larger time and spatial scales of interest (Hopmans *et al.*, 2002).

A common approach to temporal process scaling is the time-averaging of boundary conditions. This usually simplifies the calculations significantly, making it especially attractive when large-scale hydrologic systems need to be simulated. Previous studies on the effects of averaging of boundary conditions on vadose zone solute transport have been reported by Wierenga (1977), Beese and Wierenga (1980), Destouni (1991), Vanderborght *et al.* (2000), and Marshall *et al.* (2000). These studies have shown that solute transport under transient variably-saturated conditions may be approximated by a transport model with steady-state water flux and time-indifferent soil moisture content, and using a larger effective soil dispersivity to compensate for neglecting short-term moisture content variations. This effective dispersivity generally becomes depth-dependent since moisture content fluctuations typically are larger near the soil surface and decrease with soil depth. Beese and Wierenga (1980) and Destouni (1991) concluded that the discrepancy between transport models using transient and steady-state flow conditions increased if root water uptake was taken into account.

In case time-averaging does not give satisfactory results, it may still give adequate predictions of the spatial-ensemble distribution or statistical moments of the variable of interest. This observation was noted by van der Zee and Boesten (1991) in their detailed transient numerical flow and reactive transport simulations. Van der Zee and Boesten (1991) showed that a simplified transport model with time-invariant parameters may be used to estimate variations in pesticide leaching due to parameter heterogeneity. The same philosophy of simplification within the context of significant spatial heterogeneity and

parameter uncertainty in field and regional applications was demonstrated by Bresler and Dagan (1983), Chen *et al.* (1994), and Schoups and Hopmans (2002). Bresler and Dagan (1983) compared analytical with numerical transport models, to conclude that the fit between the two modeling approaches improved with increasing heterogeneity. Chen *et al.* (1994) showed that field-scale infiltration is well predicted by a Green-Ampt model, provided soil heterogeneity is accounted for. Schoups and Hopmans (2002) presented an efficient analytical solute transport model, designed for large-scale applications in the presence of large uncertainty. Other studies have shown that simple transport models can perform equally well as more complex models, when large time and space scales are involved (e.g. Jothityangkoon *et al.*, 2001; van der Linden and Woo, 2003).

In this paper, we are interested in the prediction of long-term root-zone salinity and salt load in drainage water from irrigated agricultural systems. The rate and degree of soil salinization depend on many interacting factors. The main mechanism of soil salt build-up in irrigated areas is by evapoconcentration of the soil solution by evaporation and transpiration of water (Tanji, 1990). This effect is commonly controlled by the annual-averaged leaching fraction, defined as the fraction of surface-infiltrated water that drains below the root zone (Raats, 1974; Hoffman and van Genuchten, 1983). In the presence of shallow saline water tables, capillary rise can result in periodic transport of salts upwards into the root zone. The resulting rate of soil salinization will depend on water table depth, shallow groundwater salinity, and soil type (Grismer and Gates, 1988; Grimes *et al*., 1984). The degree of soil salinization may be further affected by the precipitation and dissolution of salts, primarily gypsum and calcite (Oster and Rhoades, 1975). For example, irrigation of soils containing appreciable amounts of gypsum may dissolve these minerals, thereby increasing the salt

concentration in soil solution and drainage water. Cation exchange reactions between the soil solution and the soil exchange complex can further complicate salinity dynamics by altering the composition of cations in solution that might lead to precipitation or dissolution of soil minerals and changes in soil solution salinity (Robbins *et al.*, 1981). Moreover, Tanji (1969) demonstrated the effects of ion pairing, common ions and ionic strength on total solubility of gypsum in aqueous systems. Precipitation-dissolution of calcite, on the other hand, is strongly influenced by the partial soil CO_2 pressure. An extensive review of salt chemistry in soil-water systems was presented by Oster and Tanji (1985).

Because of the large complexity and inter-dependence of the soil processes affecting soil salinization in the longterm, it is useful to identify the main controlling processes and seek simplified process descriptions (Tanji, 1981). The objective of this study is to quantify the errors introduced by various model simplifications for the prediction of long-term root-zone salinity and drainage salt load, to be applied to regional scales. The reference benchmark case of our analysis consisted of detailed numerical simulations with the one-dimensional UNSATCHEM model (Suarez and Simunek, 1997; Simunek *et al.*, 1996), and predicts average root-zone salinity using daily boundary conditions for rain, irrigation, evaporation and transpiration rate at the highest considered level of model complexity. The benchmark simulations serve to represent irrigated fields conditions in the western San Joaquin Valley, CA. The results of model simplifications are then compared to this benchmark case. Model simplifications were related to (i) the time-scale of the boundary conditions, (ii) the level of spatial vertical discretization, and (iii) the complexity of the soil reaction system. It is implicitly assumed that the UNSATCHEM model with daily boundary conditions is valid at the local scale for simulation of the short-term dynamics of soil

salinization. This is a reasonable assumption since UNSATCHEM and other geochemical salinity models have been successfully calibrated using leaching experiments in lysimeters (Oster and Rhoades, 1975; Wierenga *et al.*, 1975; Jury *et al.*, 1978; Robbins *et al.*, 1981) and small field plots (Tanji *et al.*, 1972; Dudley *et al.*, 1981; Ali *et al.*, 2000; Suarez, 2001). We further assume that a one-dimensional representation of soil salinity dynamics is a useful starting point for the upscaling to the regional-scale using a spatial-distributed modeling approach. However, the validity of this assumption is subject to general discussion in hydrology (e.g., Hopmans et al; 2002; Wallender and Grismer, 2002). At the onset, we point out that the presented study is a model sensitivity analysis; a comparison with field data is subject to an ongoing analysis and will be reported in another publication.

Results of the benchmark simulations are discussed in detail, followed by a sensitivity analysis that evaluates the effects of the various model simplifications. The results provide insight into the relative importance of the various interacting processes affecting soil salinity and salt drainage in irrigated soils at the longterm.

METHODS

Description of the numerical model

UNSATCHEM is a one-dimensional numerical soil water flow and transport model, simulating variably-saturated flow, heat transport, CO_2 production and transport, and solute transport of 7 major ions, coupled to equilibrium and kinetic chemistry routines (Simunek *et al.*, 1996; Suarez and Simunek, 1997). In our application, we exclude heat transport as well as CO_2 production and transport processes. In theory, temperature affects the chemical

equilibria. However, preliminary runs indicated a very limited sensitivity of salinity to temperature. Furthermore, CO_2 production and transport are excluded, although under ponded conditions CO_2 accumulation may significantly affect the rate of calcite dissolution (Simunek and Suarez, 1997). Variably saturated flow is simulated with the Richards equation,

$$\frac{\partial \theta}{\partial t} = \frac{\partial}{\partial z}\left(K \frac{\partial h}{\partial z} + K \right) - r_w \qquad (1)$$

where h is the soil water pressure head (L), θ is volumetric water content (L^3/L^3), K is the unsaturated hydraulic conductivity (L/T), t is time (T), z is the spatial coordinate (positive upward) (L), and r_w defines the root water uptake term (1/T). Root water uptake is simulated as a function of depth and time, and is a function of nodal pressure head and the osmotic head values to account for water and salt stress, respectively. The root-zone depth increases linearly with time from planting to full crop development to simulate a growing crop, whereas the root distribution is taken as trapezoidal (Simunek *et al.*, 1996). The flow equation is solved numerically using a mass-lumped fully implicit Galerkin finite element method. The dependence of K and h on θ is represented by van Genuchten-Mualem type models.

Transport of 7 major ions is considered, namely Ca^{2+}, Mg^{2+}, Na^{+}, K^{+}, HCO_3^{-}, SO_4^{2-}, and Cl^{-}. Solute transport of each aqueous species is simulated with the advection-dispersion equation,

$$\frac{\partial \theta c_k}{\partial t} = \frac{\partial}{\partial z}\left(D\theta \frac{\partial c_k}{\partial z} - q c_k \right) - \rho_b \frac{\partial \overline{c_k}}{\partial t} - \rho_b \frac{\partial \overline{\overline{c_k}}}{\partial t} \qquad \forall k = 1,...,7 \qquad (2)$$

where c_k is total dissolved concentration of aqueous species k (M/L^3), $\overline{c_k}$ is total sorbed phase concentration of aqueous species k (M/M), $\overline{\overline{c_k}}$ is total solid phase concentration of aqueous species k (M/M), ρ_b is soil bulk density (M/L^3), D is the dispersion coefficient (L^2/T), q is the Darcy water flux (L/T). For conservative species (Cl^- only), the second and third terms on the right side are zero. For all the other ions, the second and third terms are determined by solving the reaction system, as discussed later. The transport equation is solved using a Galerkin finite element method with a Crank-Nicolson implicit scheme. The Darcy water flux, q, is calculated from

$$q = -K \frac{\partial h}{\partial z} - K \qquad (3)$$

The dispersion coefficient, D, represents the combined effects of mechanical dispersion and molecular diffusion,

$$D = \alpha \frac{|q|}{\theta} + D_m \tau \qquad (4)$$

where α is dispersivity (L), $|q|$ is the absolute value of the Darcy water flux (L/T), D_m is the molecular diffusion coefficient (L^2/T), and τ is tortuosity (dimensionless), calculated as a function of moisture content.

The chemical reactions include ion complexation, cation exchange, and mineral precipitation-dissolution, as summarized in Table 1. Both modified Debye-Huckel and Pitzer expressions are incorporated to calculate single ion activities. All cations in solution (Ca^{2+}, Mg^{2+}, Na^{+}, K^{+}) are assumed to be in instantaneous equilibrium with their sorbed counterparts ($\overline{Ca}, \overline{Mg}, \overline{Na}, \overline{K}$). These sorbed components balance the total net negative charge of the clay minerals and organic matter, defined by the cation exchange capacity, CEC, of the soil,

$$CEC = \overline{Ca} + \overline{Mg} + \overline{Na} + \overline{K} \tag{5}$$

where both CEC and sorbed concentrations are expressed in $mmol_c/kg$ soil. Exchange equilibria between the sorbed and dissolved cations are described by the Gapon equation,

$$K_{Mg-Ca} = \frac{(Ca)^{1/2}\,\overline{Mg}}{(Mg)^{1/2}\,\overline{Ca}} \tag{6}$$

$$K_{Ca-Na} = \frac{(Na)\,\overline{Ca}}{(Ca)^{1/2}\,\overline{Na}} \tag{7}$$

$$K_{Ca-K} = \frac{(K)\,\overline{Ca}}{(Ca)^{1/2}\,\overline{K}} \tag{8}$$

where K_{Mg-Ca}, K_{Ca-Na}, and K_{Ca-K} are defined as Gapon selectivity coefficients (dimensionless), and parentheses indicate ion activity (dimensionless). The composition and concentration of the soil solution may change by precipitation-dissolution of gypsum and calcite (Oster and Tanji, 1985). These reactions are assumed to be at equilibrium, and are characterized by mineral solubility products,

$$K_{sp}^{G} = \left(Ca^{2+}\right)\left(SO_4^{2-}\right)\left(H_2O\right)^2 \tag{9}$$

$$K_{sp}^{C*} = \frac{\left(Ca^{2+}\right)\left(HCO_3^{-}\right)^2}{\left(H_2O\right)} = K_{sp}^{C}\frac{K_{CO_2}K_{a1}P_{CO_2}}{K_{a2}} \tag{10}$$

where K_{sp}^{G} and K_{sp}^{C} are respectively the solubility product constants of gypsum and calcite (dimensionless); K_{CO_2} is Henry's law constant (dimensionless), a measure of the solubility of CO_2 in water; K_{a1} and K_{a2} are respectively the first and second dissociation constants of carbonic acid (dimensionless); and P_{CO_2} is the partial pressure of CO_2 in soil air (Pa). Although the UNSATCHEM model considers several other Mg-Ca-minerals (nesquehonite, hydromagnesite, sepiolite, and dolomite), simulations did not predict precipitation of any of these minerals, so that these will not be discussed further. Ion complexation refers to the association of cations and anions in solution, such as the complexation of Ca^{2+} and SO_4^{2-} ions to form $CaSO_4^0$,

$$Ca^{2+} + SO_4^{2-} \Leftrightarrow CaSO_4^0 \qquad K_1 = \frac{\left(Ca^{2+}\right)\left(SO_4^{2-}\right)}{\left(CaSO_4^0\right)} \qquad (11)$$

where K_1 is the equilibrium constant for the reaction (dimensionless). In a gypsum dissolving system this reaction will enhance total solubility of gypsum. Similar complexes are formed between additional cations and anions in solution, each of them characterized by an equilibrium constant (Table 1). The effects of ion complexation on the total solubility of gypsum are discussed in detail in Tanji (1969). The complete chemical model consists of a nonlinear algebraic system, which is solved iteratively using several convergence criteria as described by Simunek *et al.* (1996). Values for several chemical equilibrium constants are listed in Table 2. All other chemical constants were adopted from Simunek *et al.* (1996).

The solution of the soil reaction system gives values for the second and third terms in Eq. (2). The coupling of transport and reactions was done using an operator splitting approach (Steefel and MacQuarrie, 1996), by which the transport equation and the chemical system are solved sequentially for every time step, without iteration. This non-iterative approach may introduce numerical errors if the time-step becomes too large (Carrayrou *et al.,* 2004). Simunek and Suarez (1994) briefly discussed this issue as it relates to reactive salt transport. In a single example, they found differences in the predicted locations of calcite precipitation zones when iterations were used or not. However, they concluded that iterations may be avoided if the interest is only in aqueous concentrations.

Benchmark numerical simulations

We consider a hypothetical situation of an irrigated cotton crop, grown under conditions that are typical for the western San Joaquin Valley in California. The benchmark model (M0 in Table 5) domain consists of a one-dimensional vertical 210 cm deep soil profile, representing the crop root zone. Soil parameters to define the soil hydraulic functions (van Genuchten, 1980) are representative for a clayey soil (Table 2), widely represented in the western San Joaquin Valley (Schoups, 2004).

The domain is discretized by 234 nodes, to yield a uniform nodal spacing of a little less than 1 cm. This level of spatial discretization ensures accurate simulation of the nonlinear flow dynamics in the root-zone (van Dam and Feddes, 2000). Each simulation extends for a period of 10 years, with each year consisting of a fallow winter period, followed by the irrigated cotton crop. The upper (top) boundary conditions of rainfall, irrigation and potential evapotranspiration (*ET*) were specified on a daily basis. Daily meteorological data were taken from the Hanford weather station, located in the western San Joaquin Valley, California, for the period October 1987 to September 1988. The annual rainfall for this period was 21.3 cm. The growing season included 6 irrigation events, including a pre-irrigation, with amounts and timing representative for a furrow-irrigated cotton crop. To simplify the presented analysis, boundary conditions were repeated every year, and only a single crop was considered. Evaporation was calculated by the model, determined by the smallest of the potential evaporation rate, as controlled by atmospheric conditions, and the soil water flux at the soil surface. For the lower boundary condition we specified either gravity drainage (deep water table) or a constant zero pressure head at the 210 cm depth to represent the shallow water table condition. In the case of gravity drainage, the bottom water flux (leaching rate) is equal to the soil's hydraulic conductivity

corresponding with the simulated soil water pressure head at the 210 cm depth, and is always downwards. An initial pressure head within the soil profile was selected that corresponds with hydrostatic conditions.

The top transport boundary condition was of the Cauchy type, with specified ion concentrations for rain and irrigation (Table 3). The lower boundary was specified as a Neumann condition for the free drainage case, for which no diffusion or dispersion occurs across the lower boundary. For the shallow water table simulations we specified a Dirichlet condition with specified groundwater concentrations (Table 3). Soil solution initial conditions were assumed equal to the irrigation water concentrations. We specified uniform initial calcite and gypsum content values (see Table 2). The initial amount of gypsum was much less than calcite, in order to reduce the CPU time required to simulate the dynamics of soil gypsum removal. The soil exchange complex was assumed to be initially saturated with Ca.

Salinity was simulated with (R) and without (NR) chemical reactions for a range of leaching fractions, water table depths, groundwater salinities, and initial gypsum contents, for a total of 12 cases (Table 4). The first four cases correspond to free drainage, i.e. a deep water table and net leaching conditions, whereas cases 5 through 8 simulate a saline shallow water table at the 210 cm soil depth; yet with a positive net leaching fraction. The last four cases 9 through 12 represent a saline shallow water table, however, net capillary rise upwards prevents salt leaching. The shallow groundwater cases were repeated for two different groundwater salinities and composition (samples 1 and 2 in Table 3). Groundwater sample 1 has a moderate salinity (3,000 mg/l) and is under-saturated with respect to gypsum. In contrast, the salinity of groundwater sample 2 is much higher (8,000 mg/l) and is super-

saturated with respect to gypsum. These two Na-SO_4 rich groundwater samples are representative of shallow groundwater qualities in the western San Joaquin Valley (Deverel and Gallanthine, 1989). Simulations with samples 1 and 2 were conducted with initial gypsum content values of 10 (0.1% w/w) and 58 $mmol_c$/kg (0.5% w/w), respectively.

For each case, the two main variables of interest were average root-zone salinity, expressed as total dissolved solids or TDS (mg/l or ppm), and annual drainage salt load, S (g/m^2/year), computed from

$$TDS = \sum_{k=1}^{7} m_k \hat{c}_k \quad \text{and} \quad S = \sum_{k} m_k S_k \tag{12a}$$

where m_k is atomic or formula weight of species k (mg/mmol), $\hat{c}_k$ is the depth-averaged dissolved concentration of species k (mmol/l), and S_k is the annual solute flux of species k that drains from the bottom of the root-zone. The average root-zone concentrations were calculated from the arithmetic average of all nodal concentrations, c_k,

$$\hat{c}_k = \frac{1}{n} \sum_{j=1}^{n} c_k^j \tag{12b}$$

where n is the total number of nodes. The annual solute flux, S_k, was computed from the cumulative solute flux at the bottom of the root-zone, L, or

$$S_k = \sum_{j=1}^{n_t} \left(q c_k - D \frac{\partial c_k}{\partial z} \right)_{z=L} \qquad (12c)$$

where n_t is the number of model time steps within the simulated year. We note that S_k is negative if the salt flux is downwards and out of the root-zone. We selected average root-zone salinity and annual drainage load as the main variables, as they represent composite indicators of soil salinity dynamics and salt export, relevant for longterm salinity management practices.

Model simplifications

The benchmark simulations were used as a reference (M0 in Table 5) to quantify errors resulting from subsequent model simplifications. From this information we will identify the optimum level of model complexity that accounts for the most important processes. Simplifications (models M1 through M5 in Table 5) were introduced incrementally and are related to (1) the time-scale of the boundary conditions, (2) the level of vertical discretization, and (3) the complexity of the reaction system in Table 1. Time-averaged boundary conditions used annual-averaged values for evaporation, transpiration, and infiltration rates, as computed from the benchmark simulations. The time-averaged model uses a fixed root water uptake distribution, equal to that of the fully developed crop of the benchmark model. The boundary conditions were averaged using:

$$\bar{q} = \frac{1}{T_a} \int_0^{T_a} q(t) dt \qquad (13)$$

where $\overline{q}$ and q are the time-averaged and daily water fluxes (I = irrigation, R = rain, E = evaporation, T = transpiration, and D = drainage), respectively, and T_a is set to one year. The time-averaged concentration of the infiltrating water, C_0, was calculated from

$$\overline{C_0} = \frac{C_R \overline{R} + C_I \overline{I}}{\overline{R} + \overline{I} - \overline{E}} \tag{14}$$

where C_R and C_I are the concentrations of rain and irrigation water; $\overline{R}$, $\overline{I}$, $\overline{E}$ denote the time-averaged rain, irrigation, and evaporation, respectively, and $\overline{R} + \overline{I} - \overline{E}$ is net infiltration in the time-averaged model. Using Eq. (14) ensures that the time-averaging does not change applied solute mass. We expect though that the time-averaging removes some of the nonlinearities of the benchmark simulations caused by daily rainfall events and irrigation followed by periods of no infiltration. The lower transport boundary condition is identical between the benchmark and time-averaged simulations.

As an additional simplification we decreased the number of spatial nodes from 234 to 15. This coarser discretization with a nodal spacing of about 15 cm (M2 through M5 in Table 5) allowed much larger time steps, thereby reducing CPU time. However, we recognize that errors may be introduced if the spatial and temporal discretization steps are too large, as defined by the Peclet and Courant numbers (Zheng and Bennett, 2002). Using the criterion of Simunek *et al.* (1996) that the product of the grid Peclet and Courant numbers must be smaller than 2, the time step was automatically adjusted to ensure numerical stability and minimize numerical dispersion, Nevertheless, additional errors are

introduced with increasing time steps, since transport and reactions are solved in sequence rather than simultaneously (Steefel and MacQuarrie, 1996; Carrayrou *et al.*, 2004).

A third simplification was considered by simplifying the salt chemistry of Table 1 incrementally in three steps. First, in simulation M3 the cation exchange reactions were turned off by setting the CEC equal to 0. Second, in simulation M4 no reactions were included except for gypsum dissolution-precipitation using a constant solubility product; finally the third step (M5) does not include any chemical reactions. The approach of using a constant solubility product neglects the effects of cation exchange, ion complexation, and ionic strength on total solubility of gypsum and calcite precipitation-dissolution. The complex reaction system of Table 1 is then reduced to gypsum equilibrium precipitation-dissolution only, for which the following relations hold (gypsum-saturated soil solution):

$$K_{sp}^{G*} = \left[Ca^{2+}\right]\left[SO_4^{2-}\right] \tag{15}$$

$$\left[Ca^{2+}\right]+\left[Mg^{2+}\right]+\left[Na^{+}\right]+\left[K^{+}\right]=\left[HCO_3^{-}\right]+\left[SO_4^{2-}\right]+\left[Cl^{-}\right] \tag{15a}$$

where square brackets denote concentrations. The second equation ensures electroneutrality of the soil solution. For known concentrations of Mg, Na, K, SO_4, and Cl after solving the transport equation for each time step, the Ca concentrations are computed by solving for SO_4 from Eq. (15a) and substituting into Eq. (15) leading to the following quadratic equation:

$$\left[Ca^{2+}\right]^2+\left\{\left[Mg^{2+}\right]+\left[Na^{+}\right]+\left[K^{+}\right]-\left[HCO_3^{-}\right]-\left[Cl^{-}\right]\right\}\left[Ca^{2+}\right]-K_{sp}^{G*}=0 \tag{15b}$$

After solving for Ca, the SO_4 concentration is determined in a similar fashion using Eqs. (15a) and (15). The change in Ca concentration before and after equilibrating with gypsum yields the extent of gypsum dissolution or precipitation. In Eq. (15), K_{sp}^{G*} is the total solubility of gypsum in distilled water, i.e. 30.7 $mmol_c/l$, which accounts for the association of Ca and SO_4 ions (Tanji, 1969).

The various stepwise model simplifications implemented are summarized in Table 5. The errors due to simplification are quantified by the relative absolute difference (%) of average root-zone TDS and drainage salt load value, *S,* at the end of the 10-year simulation period, or

$$\varepsilon = 100\left|\frac{\overline{X} - X}{X}\right| \qquad (16)$$

where $\overline{X}$ is the prediction with the simplified model, and X is the daily prediction from the benchmark simulation.

RESULTS AND DISCUSSION

Benchmark simulations for different cases (M0)

The objective of the benchmark simulations is to illustrate the salinity dynamics on the short term and the long-term, using average soil salinity and drainage salt load as key

variables. Moreover, subsequent model simplifications in sections 2, 3 and 4 will be compared with the benchmark simulations, using the relative error as defined in Eq. (16). Although we have results for all 12 cases of Table 4, this section only considers cases 4, 8 and 12 (R) and their corresponding cases 3, 7 and 11 (NR). These cases correspond to a deep water table with net leaching (cases 3 and 4), a shallow water table with net leaching (cases 7 and 8), and a shallow water table with no net leaching (cases 11 and 12).

Figure 1 presents the one-year daily dynamics of the water balance components for cases 3 and 4, from October 1 to September 30. The occasional rain events I in the winter when no crop is grown cause large fluctuations in soil evaporation (E). The pre-irrigation (I) in February (Table 4) is intended to leach salts by drainage (D) that accumulated during the previous growing season and to provide favorable soil moisture conditions before planting. The cotton crop is planted in April, resulting in subsequent transpiration (T) and decreasing E, except after the first 2 irrigations when the soil is only partly covered. During the growing season, five additional 160-mm irrigations were applied to satisfy crop water requirements, resulting in significant drainage fluxes (negative). We note that the bottom water flux (D) is never upwards (positive), because of the gravity drainage boundary condition. To demonstrate the spatial resolution of the benchmark simulations, Figure 2A shows the soil moisture profiles during and after the fifth irrigation event, with soil moisture profiles before, during (0 days), and 1 and 5 days after the irrigation. The flow dynamics are summarized in Figures 2B and 2C, presenting the 10-year average and standard deviation of water flux versus soil depth. This average water flux, computed by averaging the daily water flux values for the 10 year period, increases from the land surface to the 100 cm depth. This depth corresponds to the average infiltration depth of the irrigation events and coincides

with the soil depth for which the standard deviation of the daily water fluxes decreases towards near-zero (Fig. 2C). The steady state water flux as a function of depth resulting from using time-averaged boundary conditions (as discussed in section 2) is shown for comparison: it smoothly decreases with depth due to root water uptake.

Figures 3A and 3B compares the simulated dynamics of daily average root-zone soil salinity (TDS) and cumulative annual drainage salt load (*S*) during the 10 year simulation periods for cases 3 (NR) and 4 I. The corresponding Sodium Adsorption Ratio (SAR) and soil gypsum values for the R case are presented in Figs. 3C and 3D. Considering the short time dynamics first, the pre-irrigation reduces soil salinity, each subsequent irrigation causes TDS to fluctuate, with a final significant increase in soil salinity at the end of each growing season (see inset of Fig. 3A). Considering the 10 year simulation period, for the case with reactions I, the model predicts a decrease in soil salinity over time. This slow decrease follows the initial instantaneous dissolution of gypsum at time zero, resulting in an initial soil salinity level of about 2300 mg/l that is much larger than the irrigation water TDS (308 mg/l, Table 3). As irrigation proceeds, irrigation with gypsum-undersaturated water gradually leaches the gypsum (Fig. 3D) and decreases soil salinity (Fig. 3A). Continuing the simulations beyond the 10 year period will result in additional leaching of gypsum and a soil salinity level, similar to the non-reactive (NR) case. Simulation results show that for the gypsum-undersaturated irrigation water, gypsum dissolution is the main contributor to soil salinity for deep water table conditions, and is much more important than calcite because of its much higher solubility. Naturally, irrigation with waters with higher concentrations of Ca and SO_4 ions will result in less gypsum dissolution. We also note that elevated CO_2 concentrations that can develop under ponded conditions, can significantly increase the

solubility of calcite (Simunek and Suarez, 1997). Because of the significant gypsum dissolution, also the drainage salt load, *S*, (Fig. 3B) is larger (more negative) than the corresponding non-reactive (NR) case. Finally, since the simulations start with an initially Ca-saturated sorption complex, the subsequent exchange of sorbed Ca by Na of the rainfall and irrigation water gradually increases the SAR (Fig. 3C) during the simulation period.

The flow dynamics for cases 7 and 8 are presented in Figure 4. With everything else being the same, the only difference for these cases is that the bottom boundary condition changed from a free drainage to a constant 210 cm deep water table. This change in boundary condition affects the bottom water flux (Fig. 4) in two ways. First, the now much wetter soil profile reduces soil water storage thereby increasing soil water fluxes and drainage fluxes after irrigation events. Second, the water table provides for periodic upward water flow by capillary rise between irrigation events. The resulting water flux variations cause within-year fluctuations of average root-zone salinity (TDS) that are much larger than the previous case (compare Fig. 5A with Fig. 3A). Furthermore, the capillary rise of water and salts from the saline water table leads to the mixing of infiltration and ground waters, causing an increase in the final soil salinity level. Much of the TDS dynamics is the result of irrigating with low-saline surface water, followed by capillary rise with corresponding salinity increases between irrigation events. The input of saline groundwater is evident in Fig. 5B, which shows a net input of 10,000 g/m^2/yr. So, even though net leaching occurs on an annual basis, the upward movement of water and salts from the saline shallow groundwater leads to a significant net input of salts into the root-zone. This causes precipitation, thereby lowering TDS about equal to the NR case since the shallow groundwater is super-saturated with gypsum (Fig. 5D). For the corresponding non-reactive

case, the salt input is much less (Fig. 5B) because salts that enter the root-zone between irrigation events by capillary rise are leached down during subsequent irrigations, rather than precipitation of gypsum as in the R case. This periodic change in salt flux direction is the reason for the much larger soil salinity dynamics for the NR case in Fig. 5A. Finally, the large *Na* concentrations in the shallow groundwater result in root-zone SAR values that are much larger than for the deep water table case in Fig. 5C.

The boundary conditions for case 11 (NR) and 12 (R) are presented in Figure 6. For this set of benchmark cases, all irrigation amounts were reduced to 100 mm, thereby simulating deficit irrigation conditions leading to negative leaching (annual net upward flow). The bottom boundary consisted of a fixed water table. As in the previous case, the reduced irrigations caused significant upward fluxes (positive value for *D*), both between irrigation events and non-growing season. The resulting effects on soil salinization are shown in Figure 7. The total net water flux at the bottom of the root-zone is upwards, resulting in zero leaching of salts, leading to very high TDS levels (Fig. 7A). This clearly illustrates the need for maintaining a salt balance in the root zone by periodically leaching of salts. The salt load is consistently positive, directed upwards into the root-zone, resulting in an annual salt influx of about 8,000 $g/m^2/yr$ after a few years (Fig. 7B). Comparing annual average advective flux from the saline (sample 2) shallow water table with computed diffusive transport shows that the upward salt flux is dominated by diffusion and dispersion accounting for about 6,000 $g/m^2/yr$. This large salt mass is controlled by continuous precipitation of the incoming salts. For the R case, significant buffering of root-zone salinity occurs by precipitation of gypsum (Fig. 7D), thereby decreasing TDS as in Fig. 7A. The predicted *SAR* values are large and increasing with time due to the inflow of Na-rich

groundwater and the precipitation of Ca as gypsum. In summary, the results in Figure 7 show that salt build up for the no leaching case may eventually limit crop productivity, when gypsum precipitation is not accounted for. For example, for a cotton crop the yield-reduction threshold at field moisture conditions was set at 15 dS/m or about 12,000 mg/l, which is attained after 5 years for the NR case in Fig. 7A. The resulting salt stress reduces crop transpiration and increases leaching leading to a reduction in soil salinity. This scenario suggests that the no net leaching case may eventually attain a steady-state salinity level that is controlled by crop salt tolerance. However, in the simulations performed here salinity stress was not taken into account.

For each of the 12 cases, the first column in Tables 6 and 7 lists the benchmark simulation results of TDS and *S*, respectively. The other 5 columns present the TDS (Table 6) and *S* (Table 7) simulation results for the model simplifications M1 through M5, with the absolute error in percent between parentheses.

Effects of annually averaging the boundary conditions (M1)

The third column in Tables 6 and 7 compares TDS *and* S, using annual-averaged boundary conditions for the corresponding benchmark cases in the second column. The magnitude of the relative errors varies between near zero and 42 %. A comparison of the TDS values for cases 1 through 8 (Table 4) indicates that there is a consistent under-prediction or bias by the time-averaged model. In contrast, for cases 9 through 12 with no net leaching, the time-averaged model slightly over-predicts TDS. We explain the under-prediction for the first 8 cases by the omission of the water flux direction changes for the time-averaged model that uses the simplified averaged net downward flux at all times,

thereby underestimating the mixing of soil solution by dispersion as caused by changes in soil water flow direction during and between irrigation events (e.g. capillary rise, root water uptake and redistribution). This underestimation is expected to be largest for cases 5-8 with the shallow groundwater table, with errors of about 25-40 %. The results in Table 6 also show that the error increases as the groundwater salinity increases (compare cases 5 and 6 (low salinity) with cases 7 and 8 (high salinity), confirming that the error is controlled by the omission of upward salt transport in the M1 simulations.

The less straightforward predictions of annual salt drainage load, *S*, after 10 years are presented in Table 7. For the first 4 cases (deep water table), the errors of the time-averaged model are very small (< 4%). For cases 5-8 (shallow water table with net leaching) the errors are somewhat larger for cases 5-7 (16-19%) and very large for case 8 (99%). The net salt flux is downwards in cases 5-7, as indicated by the negative value for S. Since the time-averaged model under-estimates upward dispersion of salts from the shallow water table, it over-predicts the net downward salt flux. However for case 8, the net salt flux is upward into the root-zone due to the influx of saline shallow groundwater into the root-zone and subsequent gypsum precipitation, as discussed earlier. Therefore, the time-averaged model under-predicts the upward salt flux for case 8 causing the large error.

Similarly, the M1 model simulations for cases 9-12 (no net leaching) under-estimate periodic downward flow, thereby slightly overestimating root-zone salinity, as shown in Table 6. The time-averaged model predicts salt drainage load quite well for cases 9-11, however, for case 12 the time-averaged model under-estimates upward mixing and dispersion by 72% (Table 7). This leads to reduced gypsum precipitation and a slight over-estimation of root-zone TDS as compared to the benchmark simulations. The comparison

between the reactive I and non-reactive (NR) cases show that the errors of TDS prediction are generally lower when reactions are considered. The reaction effect on *S* in Table 7 is not so clear.

This discussion suggests that the application of a larger effective dispersivity value may reduce the bias between daily and time-averaged models, as was also suggested by Wierenga (1977) and Suarez and van Genuchten (1980). However, it is not clear how to compute these effective values for time averaging based from the short-term dynamics of daily simulations. Whereas for simpler situations closed-form expressions may be derived for the effective dispersivity (see e.g. Goode and Konikow (1990) for an application in groundwater transport), no general expressions are available for the more general nonlinear case of solute transport for transient variably-saturated flow conditions with root water uptake. Alternatively, one may estimate an effective dispersivity value using inverse procedures.

Effects of vertical discretization (M2)

At the next simplification level, the vertical discretization of the time-averaged model was decreased from 234 to 8 nodes, corresponding to a nodal spacing of about 1 to 15 cm, respectively. Differences in relative errors between the time-averaged models with fine (M1) and coarse discretization (M2) reflect errors in vertical resolution. Results in Table 6 and 7 show that predictions between the two discretization levels were similar. The main effect of a coarser discretization is a stepwise rather than continuous dissolution of gypsum, resulting in corresponding step-changes in root-zone salinity. This is illustrated in Fig. 8, showing simulated values for the average root-zone TDS of case 4 for three different

discretization levels. This discrete behaviour is caused by the assumption of instantaneous equilibrium of the gypsum dissolution-precipitation reaction during steady state flow. As a result of this model assumption, the soil solution within a grid cell will remain saturated with gypsum until all gypsum has been removed, at which point the salinity of the soil solution will change. The number and magnitude of the steps are directly related to the level of vertical discretization. It is also expected that the magnitude of the error steps is a function of the amount of initial gypsum and the rate of gypsum dissolution (which depends on the flow rate and the degree of under-saturation of the infiltrating water). This may be illustrated by the following simple example. Consider a one-dimensional uniform column containing an amount of gypsum (G) such that the initial soil solution is at a concentration c_G in equilibrium with gypsum. At time $t = 0$, the column is leached under piston flow conditions with a gypsum under-saturated solution c_0 flowing at a steady state rate q_0. Now suppose that the column is discretized into n compartments, so that each compartment contains an initial amount of gypsum equal to G/n, and the time needed to dissolve all gypsum from a single compartment equals $\frac{G}{nq_0(c_G - c_0)}$. In other words, the time to remove gypsum is longer for smaller values of the leaching rate q_0, for less under-saturated leaching solutions, and for a larger initial gypsum amount. Under the assumption that gypsum dissolution is instantaneous, the concentration c_i in each compartment equals c_G as long as gypsum is still present, and drops to c_0 once all gypsum has been removed from the compartment. Therefore, as leaching continues, the average concentration of the column will

decrease over time in a stepwise manner, where the length of each step is given by $\frac{G}{nq_0(c_G - c_0)}$ and the height of each step is given by $\frac{c_G - c_0}{n}$.

Effects of simplifying salt chemistry (M3, M4, and M5)

In addition to model simplifications M1 and M2, the benchmark simulations were compared with those that simplified the complex salt chemistry of Table 1. The simplification included three steps. In the first step (M3), the chemistry model excluded cation exchange reactions. The second simplification (M4) considered only gypsum dissolution-precipitation using a constant total solubility of gypsum in distilled water of 30.7 $mmol_c/l$, whereas the final simplification (M5) did not include any chemical reactions. These results are summarized in Tables 6 and 7. We note that the comparison is only useful for the R cases for which chemistry in the benchmark simulations is included.

Comparing the relative errors of M3 with the M2 simulations, there are small differences for cases 1-8, but a significant over-estimation (69 and 175 %) for cases 10 and 12. For the corresponding high saline Na-rich shallow groundwater cases, the neglect of cation exchange of Ca by Na results in an under-estimation of gypsum precipitation as would occur in the absence of cation exchange. For cases 5-8 (shallow water table with net leaching), the under-estimation of dispersion caused by the time-averaging of the boundary conditions was partly compensated for by an over-estimation of gypsum dissolution as caused by neglecting cation exchange. Drainage salt load was generally only slightly affected by cation exchange reactions (Table 7). In summary, cation exchange may significantly influence root-zone TDS by affecting the precipitation/dissolution of gypsum

(Robbins *et al.*, 1980). The error magnitude will depend on cationic composition differences between the sorption complex and the infiltrating soil solution. Therefore, cases 10 and 12 deviate extremely since we assumed that the soil complex was Ca-saturated initially.

The results in Tables 6 and 7 show that the next level of simplification (M4) by ignoring calcite precipitation-dissolution, ionic strength and ion complexation reactions yields nearly identical results to M3 and M2. Therefore, we conclude that inclusion of cation exchange reactions is more important when predicting rootzone salinity than considering calcite and ion complexation. Because the solubility of calcite is much lower solubility than gypsum, K_{sp} of 10^{-9} versus 10^{-5}, calcite plays a secondary role in soil salinity. Finally, the M5 (NR) simulation results in the last column of Table 6 demonstrate the high importance of accounting for gypsum dissolution-precipitation, as errors are as large as 50 % (case 4) by ignoring dissolution, and larger than 200 % (case 12) by eliminating gypsum precipitation.

Model complexity and parameter uncertainty

Intuitively, model simplification is acceptable as long as it leads to model errors that are negligible relative to errors due to parameter uncertainty as a result of spatial heterogeneity. In this section we include parameter uncertainty by spatial distributing selected cases to represent spatial variations in boundary conditions and soil chemistry of an irrigated agricultural field.

Specifically, we consider three hypothetical fields, with different assigned levels of randomly-distributed heterogeneity, as defined in Table 8. The fields 1 through 3 are composed of different combinations of the cases (cases 1, 2, 5, 6, 9, and 10 of Table 4), with the areal fractions of each case and field listed in Table 8. The homogeneous case is

represented by Field 1 with parameter values represented by case 5 (shallow water table with net leaching and no soil gypsum). Field 2 is slightly heterogeneous, with half of the field containing gypsum (case 6). Finally, Field 3 is the most heterogeneous with variations in leaching, gypsum content, and water table depth, represented by areal fractions of all 6 cases in Table 8. From the benchmark model simulations, weighted averages and ranges after the 10-year simulation period were computed from

$$AVERAGE\{TDS\} = \sum_i f_a(i) TDS(i) \tag{17a}$$

$$RANGE\{TDS\} = Max\{TDS\} - Min\{TDS\} \tag{17b}$$

where TDS(i) is the average root-zone salinity for case *i*, *i* = 1, . . .,6, and $f_a(i)$ denotes the areal fraction of case *i* for each of the 3 fields. The *AVERAGE* values for each of the 3 fields were also computed using the time-averaged model (M2). The error of the M2 simulations, relative to the benchmark simulations for each of the 3 fields, using Eq. (16) are presented in Figure 9 for Fields 1 (homogeneous), 2 (slightly heterogeneous) and 3 (highly heterogeneous). The results show that the relative model error caused by the time-averaging of the boundary conditions decreases as the field heterogeneity increases. Most likely this is caused by the compensating over-prediction and under-prediction errors. We conclude that the time-averaging of boundary conditions is acceptable when simulating long-term soil salinization. The simplified approach is even more justified for regional applications where uncertainty of model parameters is large.

SUMMARY AND CONCLUSIONS

This study investigated the effects of various model simplifications on the prediction of long-term salt transport and soil salinity in irrigated soils. Benchmark simulations using a detailed one-dimensional numerical flow and transport model that accounts for crop growth, advection, dispersion, diffusion, and complex salt chemistry, predicted daily average root-zone salinity and cumulative annual drainage salt load for a 10-year period. Benchmark simulations were conducted for 12 different cases, representing variations in water table depth, groundwater salinity, leaching fraction, soil gypsum content, and soil chemistry. Various levels of model simplification were systematically compared with the benchmark simulations, specifically by (i) time-averaging of the boundary conditions, (ii) decreasing vertical discretization, and (iii) reducing the complexity of the salt reaction system.

We conclude that prediction errors of root-zone salinity and drainage salt load by time-averaging the boundary conditions range were relatively small, except for those cases were groundwater salinity is high and both periods of upward and downward water flow occur in the presence of soil gypsum. Reducing the vertical spatial resolution of the benchmark model from 234 to 15 nodes, with corresponding nodal spacings of 1 and 15 cm respectively, did not affect the model results, except that the long term changes of annual rootzone TDS were more discrete for the coarser grid spacing because of the instantaneous equilibrium assumption of the gypsum dissolution-precipitation reaction. Eliminating cation exchange reactions and gypsum reactions significantly affected the shallow high saline

groundwater cases. However, calcite precipitation-dissolution and ion complexation reactions were found to be of minor importance.

It is concluded that the daily model using a fine vertical discretization and complex salt chemistry can be replaced in many cases by a much simpler transport model that uses annually-averaged boundary conditions, a coarse spatial discretization, and one that accounts for gypsum dissolution-precipitation only. We also demonstrated that prediction errors due to these model simplifications may be small, when compared to effects of parameter uncertainty on model predictions.

Acknowledgements

The authors acknowledge financial support by the USDA Fund for Rural America, project no. 97-36200-5263, and the scientific contributions by the principal investigators Drs. W.W. Wallender, T.C. Hsiao, S.L. Ustin, R.E. Howitt, T.H. Harter, and G.E. Fogg. We also thank Dr. D.L. Suarez for providing us with the UNSATCHEM software.

References

Ali R, Elliott RL, Ayars JE, Stevens EW. 2000. Soil salinity modeling over shallow water tables I: validation of LEACHC. *J. Irrig. Drain. Eng.* **126**: 223-233.

Beese F, Wierenga PJ. 1980. Solute transport through soil with adsorption and root water uptake computed with a transient and a constant-flux model. *Soil Sci.* **129**: 245-252.

Biggar J, Nielsen DR. 1976. Spatial variability of the leaching characteristics of a field soil. *Water Resour. Res.* **12**: 78-84.

Bresler E., Dagan G. 1983. Unsaturated flow in spatially variable fields: 3. Solute transport and their application to two fields. *Water Resour. Res.* **19**: 429-435.

CA-DWR. 1990. Water quality data of the California Aqueduct. California Department of Water Resources.

Carrayrou J., Mose R, Behra P. 2004. Operator-splitting procedures for reactive transport and comparison of mass balance errors. *J. Contam. Hydrol.* **68**: 239-268.

Chen ZQ, Govindaraju RS, Kavvas ML. 1994. Spatial averaging of unsaturated flow equations under infiltration conditions over areally heterogeneous fields: 1. Development of models. *Water Resour. Res.* **30**: 523-533.

Destouni G. 1991. Applicability of the steady-state flow assumption for solute advection in field soils. *Water Resour. Res.* **27**: 2129-2140.

Deverel SJ, Gallanthine SK. 1989. Relation of salinity and selenium in shallow groundwater to hydrologic and geochemical processes, western San Joaquin Valley, California. *J. Hydrol*. **109**: 125-149.

Dudley LM, Wagenet RJ, Jurinak JJ. 1981. Description of soil chemistry during transient solute transport. *Water Resour. Res.* **17**: 1498-1504.

1 Fetter CW. 1999. Contaminant hydrogeology, *Macmillan*, New York.
2 Goode DJ, Konikow LF. 1990. Apparent dispersion in transient groundwater flow. *Water*
3 *Resour. Res.* **26**: 2339-2351.
4 Grimes DW, Sharma RL, Henderson DW. 1984. Developing the resource potential of a
5 shallow water table. *UC Water Resour. Center* Contribution no.188.
6 Grismer ME, Gates TK. 1988. Estimating saline water table contributions to crop water use
7 for irrigation-drainage system design. *California Agriculture* **42**: 23-24.
8 Hoffman GJ, van Genuchten MTh. 1983. Soil properties and efficient water use: water
9 management for salinity control. In: *Limitations to efficient water use in crop*
10 *production*, Taylor HM, Jordan WR, Sinclair TR (eds). American Society of Agronomy:
11 Madison, Wisconsin**;** xix, 538.
12 Hopmans JW, Nielsen DR, Bristow KL. 2002. How useful are small-scale soil hydraulic
13 property measurements for large-scale vadose zone modeling. In: *Heat and mass*
14 *transfer in the natural environment, The Philip Volume*. Smiles D, Raats PAC, Warrick
15 A (eds). AGU Geophysical Monograph Series No. 129, pages 247-258.
16 Jothityangkoon C, Sivapalan M, Farmer DL. 2001. Process controls of water balance
17 variability in a large semi-arid catchment: downward approach to hydrological model
18 development**.** *J. Hydrol.* **254**: 174-198.
19 Jury WA, Frenkel H, Fluhler H, Devitt D, Stolzy LH. 1978. Use of saline irrigation waters
20 and minimal leaching for crop production. *Hilgardia* **46**: 170-192.
21 Jury WA, Gardner WR, Gardner WH. 1991. Soil physics. *John Wiley*, New York, NY.
22 Marshall JD, Shimada BW, Jaffe PR. 2000. Effect of temporal variability in infiltration on
23 contaminant transport in the unsaturated zone. *J. Contam. Hydrol.* **46**: 151-161.

NADP, National Atmospheric Deposition Program, 2003.

Oster JD, Rhoades JD. 1975. Calculated drainage water compositions and salt burdens resulting from irrigation with river waters in the Western United States. *J. Environ. Qual.* **4**: 73-79.

Oster JD, Tanji KK. 1985. Chemical reactions within the root zone of arid zone soils. *J. Irr. Drain. Eng.* **111**: 207-217.

Raats PAC. Steady flows of water and salt in uniform soil profiles with plant roots. *Soil Sci. Soc. Am. Proc.* **38**: 717-722.

Robbins CW, Wagenet RJ, Jurinak JJ. 1980. A combined salt transport-chemical equilibrium model for calcareous and gypsiferous soils. *Soil Sci. Soc. Am. J.* **44**: 1191-1194.

Schaap MG, Leij FJ, van Genuchten MTh. 1998. Neural network analysis for hierarchical prediction of soil water retention and saturated hydraulic conductivity. *Soil Sci. Soc. Am. J*. **62**: 847-855.

Simunek J, Suarez DL, Sejna M. 1996. The UNSATCHEM software package for simulating one-dimensional variably saturated water flow, heat transport, carbon dioxide production and transport, and multi-component solute transport with major ion equilibrium and kinetic chemistry. *US Salinity Laboratory, Research Report* No. 141.

Simunek J, Suarez DL. 1997. Sodic soil reclamation using multi-component transport modeling. *J. Irr. Drain. Eng.* **123**: 367-376.

Simunek J, Suarez DL. 1994. Two-dimensional transport model for variably saturated porous media with major ion chemistry. *Water Resour. Res.* **30**: 1115-113.

1 Schoups G, Hopmans JW. 2002. Analytical model for vadose zone solute transport with root
2 water and solute uptake. *Vadose Zone J.* **1**: 158-171.
3 Schoups, 2004. Regional scale hydrologic modeling of subsurface water flow and reactive
4 salt transport in the western San Joaquin Valley, CA. PhD Thesis. University of
5 California, Davis. Dept LAWR, 123 Veihmeyer Hall, Davis, CA 95616.
6 Steefel CI, MacQuarrie KTB. 1996. Approaches to modeling of reactive transport in porous
7 media. In: *Reactive transport in porous media*, Lichtner PC, Steefel CI, Oelkers EH
8 (eds). Reviews in Mineralogy **34**: 101-129.
9 Suarez DL, van Genuchten MTh. 1980. Leaching and water-type effects on groundwater
10 quality. *J. Irrig. Drain. Div. Proc. ASCE* **107**: 35-52.
11 Suarez DL, Simunek J. 1997. UNSATCHEM: Unsaturated water and solute transport model
12 with equilibrium and kinetic chemistry. *Soil Sci. Soc. Am. J.* **61**: 1633-1646.
13 Suarez DL. 2001. Sodic soil reclamation: modeling and field study. *Australian Journal of*
14 *Soil Research* **39**: 1225-1246.
15 Tanji KK. 1969. Solubility of gypsum in aqueous electrolytes as affected by ion association
16 and ionic strengths up to 0.15 M and at 25 ˚C. *Environ. Sci. Tech.* **3**: 656-661.
17 Tanji KK, Doneen LD, Ferry GV, Ayers RS. 1972. Computer simulation analysis on
18 reclamation of salt-affected soils in the San Joaquin Valley, California. *Soil Sci. Soc.*
19 *Am. Proc.* **36**: 127-133.
20 Tanji KK. 1981. River basin hydro-salinity modeling. *Agric. Water Manag.* **4**: 207-225.
21 Tanji KK. 1990. Nature and extent of agricultural salinity. In: *Agricultural salinity*
22 *assessment and management*, Tanji KK (ed). ASCE Manuals and Reports on
23 Engineering Practice no.71.

van Dam JC, Feddes RA. 2000. Numerical simulation of infiltration, evaporation, and shallow groundwater levels with the Richards equation. *J. Hydrol.* **233**: 72-85.

Vanderborght J, Jacques D, Feyen J. 2000. Deriving transport parameters from transient flow leaching experiments by approximate steady-state flow convection-dispersion models. *Soil Sci. Soc. Am. J.* **64**: 1317-1327.

Van der Linden S, Woo M. 2003. Application of hydrological models with increasing complexity to subarctic catchments. *J. Hydrol.* **270**: 145-157.

Van der Zee SEATM, Boesten JJTI. 1991. Effects of soil heterogeneity on pesticide leaching to groundwater. *Water Resour. Res.* **27**: 3051-3063.

van Genuchten, M.Th. (1980). A Closed-Form Equation for Predicting the Hydraulic Conductivity of Unsaturated Soils. *Soil Sci. Soc. Am. J.*, **44**:892-898.

Wallender, W.W., and M.E. Grismer. 2002. Irrigation Hydrology: Crossing scales. *J. Irrig. and Drainage Eng.***128**:203-211.

Wierenga PJ, Shaffer MJ, Gomez SP, O'Connor GA. 1975. Predicting ionic distributions in large soil columns. *Soil Sci. Soc. Am. Proc.* **39**: 1080-1084.

Wierenga PJ. 1977. Solute distribution profiles computed with steady-state and transient water movement models. *Soil Sci. Soc. Am. J.* **41**: 1050-1055.

Zheng C, Bennett GD. 2002. Applied contaminant transport modeling. *John Wiley & Sons*, New York, 621 pages.

Table 1 – Chemical reactions considered by UNSATCHEM (Simunek *et al.*, 1996). All reactions are in instantaneous equilibrium. Chemical species with a bar denote sorbed species. The "*" in $H_2CO_3^*$ indicates a species of low stability.

Reaction	Equilibrium constant
CO_2-H_2O system	
$H_2O \Leftrightarrow H^+ + OH^-$	K_w
$CO_2(g) + H_2O \Leftrightarrow H_2CO_3^*$	K_{CO_2}
$H_2CO_3^* \Leftrightarrow H^+ + HCO_3^-$	K_{a1}
$HCO_3^- \Leftrightarrow H^+ + CO_3^{2-}$	K_{a2}
Ion pairing (complexation)	
$CaSO_4^0 \Leftrightarrow Ca^{2+} + SO_4^{2-}$	K_1
$CaCO_3^0 \Leftrightarrow Ca^{2+} + CO_3^{2-}$	K_2
$CaHCO_3^+ \Leftrightarrow Ca^{2+} + HCO_3^-$	K_3
$MgSO_4^0 \Leftrightarrow Mg^{2+} + SO_4^{2-}$	K_4
$MgCO_3^0 \Leftrightarrow Mg^{2+} + CO_3^{2-}$	K_5
$MgHCO_3^+ \Leftrightarrow Mg^{2+} + HCO_3^-$	K_6
$NaSO_4^- \Leftrightarrow Na^+ + SO_4^{2-}$	K_7
$NaCO_3^- \Leftrightarrow Na^+ + CO_3^{2-}$	K_8
$NaHCO_3^0 \Leftrightarrow Na^+ + HCO_3^-$	K_9
$KSO_4^- \Leftrightarrow K^+ + SO_4^{2-}$	K_{10}
Cation exchange reactions	
$\frac{1}{2}Ca^{2+} + \overline{Mg} \Leftrightarrow \overline{Ca} + \frac{1}{2}Mg^{2+}$	K_{Mg-Ca}
$\frac{1}{2}Ca^{2+} + \overline{Na} \Leftrightarrow \overline{Ca} + Na^+$	K_{Ca-Na}
$\frac{1}{2}Ca^{2+} + \overline{K} \Leftrightarrow \overline{Ca} + K^+$	K_{Ca-K}
$\frac{1}{2}Mg^{2+} + \overline{Na} \Leftrightarrow \overline{Mg} + Na^+$	K_{Mg-Na}
$\frac{1}{2}Mg^{2+} + \overline{K} \Leftrightarrow \overline{Mg} + K^+$	K_{Mg-K}
$Na^+ + \overline{K} \Leftrightarrow \overline{Na} + K^+$	K_{Na-K}
Precipitation-dissolution	
$CaSO_4.2H_2O(s) \Leftrightarrow Ca^{2+} + SO_4^{2-} + 2H_2O$	K_{sp}^G
$CaCO_3(s) + CO_2(g) + H_2O \Leftrightarrow Ca^{2+} + 2HCO_3^-$	K_{sp}^C

1 Table 2 – Overview of parameter values used in the UNSATCHEM simulations

Parameter	Value	Unit	Reference or Comment
soil bulk density	1.4	g/cm^3	Jury *et al.* (1991)
Hydraulic parameters for clay			Schaap *et al.* (1998)
K_s	14.8	cm/day	
α	0.015	1/cm	
n	1.25	-	
θ_r	0.10	-	
θ_s	0.46	-	
molecular diffusion coefficient	10^{-5}	cm^2/s	Fetter (1999)
dispersivity	8.3	cm	Biggar and Nielsen (1976)
Cation exchange coefficient	350	$mmol_c/kg$	Jury *et al.* (1990)
Gapon selectivity coefficients			
K_{Mg-Ca}	0.63	-	Robbins *et al.* (1980)
K_{Ca-Na}	6.3	-	Robbins *et al.* (1980)
K_{Ca-K}	0.36	-	Robbins *et al.* (1980)
Gypsum solubility, K_{sp}^{G} (20° C)	$2.5\ 10^{-5}$	-	Simunek *et al.* (1996)
Calcite solubility, K_{sp}^{C} (20° C)	$3.5\ 10^{-9}$	-	Simunek *et al.* (1996)
Soil temperature	20°	C	Constant in time
CO_2 content	0.00033 (top) 0.02 (bottom)	vol%	Constant in time
Initial dissolved concentrations	Irrigation water		Table 3
Initial sorbed concentrations ($\overline{Ca}/\overline{Mg}/\overline{Na}/\overline{K}$)	350/0/0/0	$mmol_c/kg$ soil	
Initial calcite	400	$mmol_c/kg$	
Initial gypsum	10 or 58	soil	
Annual rainfall	213	mm/yr	
Annual potential *ET*	927	mm/yr	
Number of irrigation events	6		
Irrigation amount (by event)	160/160/100	mm	

2

1

2 Table 3 – Salinity and composition of rain, irrigation, and shallow groundwater

Variable	Unit	Rain	Irrigation water	Shallow groundwater	
				Sample 1	Sample 2
Ca	$mmol_c/l$	0.002	0.998	14.5	28.44
Mg	$mmol_c$ /l	0.0032	1.234	9.0	15.63
Na	$mmol_c$ /l	0.0183	2.54	31.0	86.99
K	$mmol_c$ /l	0.0005	0.0	0.0	0.18
HCO_3	$mmol_c$ /l	0.005	0.822	2.82	3.5
SO_4	$mmol_c$ /l	0.009	1.10	30.0	108.85
Cl	$mmol_c$ /l	0.01	2.85	21.68	18.89
SAR*	$(mmol_c/l)^{0.5}$	0.36	2.40	9.04	18.53
TDS	mg/l	1.61	308.0	3494.3	8878.4
Reference		NADP (2003)	CA-DWR (1990)	Deverel and Gallanthine (1989)	

3 * $SAR = \frac{Na}{\sqrt{\frac{Ca + Mg}{2}}}$

Table 4 – Parameter values for the different cases.

Case	Water table depth (cm)	Net leaching	Irrigation amount per event (mm)	Initial gypsum ($mmol_c/kg$)	Groundwater salinity	Reactions
1	Free drainage	Yes	160	10	-	NR
2	Free drainage	Yes	160	10	-	R
3	Free drainage	Yes	160	58	-	NR
4	Free drainage	Yes	160	58	-	R
5	210	Yes	160	10	Sample 1	NR
6	210	Yes	160	10	Sample 1	R
7	210	Yes	160	58	Sample 2	NR
8	210	Yes	160	58	Sample 2	R
9	210	No	100	10	Sample 1	NR
10	210	No	100	10	Sample 1	R
11	210	No	100	58	Sample 2	NR
12	210	No	100	58	Sample 2	R

1 Table 5 – Summary of different models with increasing levels of simplification.

Level of model simplification	Boundary conditions	Nodal spacing (cm)	Cation exchange	Calcite dissolution-precipitation	Ion complexation	Gypsum dissolution-precipitation
M0 - Unsatchem	Daily	1	Yes	Yes	Yes	Yes
M1	Annual	1	Yes	Yes	Yes	Yes
M2	Annual	15	Yes	Yes	Yes	Yes
M3	Annual	15	No	Yes	Yes	Yes
M4	Annual	15	No	No	No	Yes
M5	Annual	15	No	No	No	No

2

3

4

Table 6 – Predicted root-zone average TDS (mg/l) and relative errors (%) after 10 years between daily model (M0) and different models using increasing levels of simplification, as defined in Table 5. The different cases are summarized in Table 4. Errors larger than 50% are highlighted in bold face.

	Level of model complexity					
Case	M0	M1	M2	M3	M4	M5
1	1132	944 (17)	943 (17)	943 (17)	943 (17)	943 (17)
2	1093	978 (11)	973 (11)	1041 (5)	943 (14)	943 (14)
3	1130	944 (16)	943 (17)	943 (17)	943 (17)	943 (17)
4	2046	1859 (9)	1864 (9)	1982 (3)	1909 (7)	943 (54)
5	2015	1546 (23)	1570 (22)	1570 (22)	1570 (22)	1570 (22)
6	1970	1717 (13)	1776 (10)	1663 (16)	1853 (6)	1570 (20)
7	3460	2012 (42)	2176 (37)	2176 (37)	2176 (37)	2176 (37)
8	3410	2547 (25)	2731 (20)	2963 (13)	2814 (17)	2176 (36)
9	11079	12038 (9)	12463 (13)	12463 (13)	12463 (13)	12463 (13)
10	5972	6511 (9)	6619 (11)	**10114 (69)**	**9759 (63)**	**12463 (109)**
11	26219	26141 (0)	27636 (5)	27636 (5)	27636 (5)	27636 (5)
12	8278	8690 (5)	9032 (9)	**22775 (175)**	**21976 (165)**	**27636 (234)**

Table 7 – Predicted annual drainage salt load S (g/m^2/yr) and relative errors (%) after 10 years between daily model (M0) and different models using increasing levels of simplification, as defined in Table 5. The different cases are summarized in Table 4. Errors about equal or larger than 50% are highlighted in bold face.

	Level of model complexity					
Case	M0	M1	M2	M3	M4	M5
1	-278	-288 (4)	-288 (4)	-288 (4)	-288 (4)	-288 (4)
2	-275	-279 (1)	-283 (3)	-307 (12)	-289 (5)	-288 (5)
3	-279	-288 (3)	-288 (3)	-288 (3)	-288 (3)	-288 (3)
4	-566	-564 (0)	-563 (0)	-653 (15)	-607 (7)	-288 (49)
5	-248	-287 (16)	-288 (16)	-288 (16)	-288 (16)	-288 (16)
6	-374	-444 (19)	-432 (16)	-430 (15)	-450 (20)	-288 (23)
7	-245	-287 (17)	-290 (18)	-290 (18)	-290 (18)	-290 (18)
8	10730	**160 (99)**	**-111 (101)**	**-280 (103)**	**214 (98)**	**-290 (103)**
9	692	765 (11)	767 (11)	767 (11)	767 (11)	767 (11)
10	615	658 (7)	743 (21)	743 (21)	767 (25)	767 (25)
11	1770	1944 (10)	1948 (10)	1948 (10)	1948 (10)	1948 (10)
12	7964	**2214 (72)**	**2029 (75)**	**2014 (75)**	**2196 (72)**	**1948 (76)**

Table 8. Areal fraction of specific case, $f_a(i)$, for Fields 1, 2 and 3, and computed weighted average and range of TDS.

Case of Table 4	*i*			
		Field 1	Field 2	Field 3
1	1	0	0	0.2
2	2	0	0	0.2
5	3	1	0.5	0.2
6	4	0	0.5	0.2
9	5	0	0	0.1
10	6	0	0	0.1
AVERAGE{TDS}		2054	2012	2967
RANGE{TDS}		0	42	3044

Figure Captions

Figure 1 Daily water balance for one year for the case of deep water table (cases C1-C4).

Figure 2 (A) Soil moisture dynamics following an irrigation event, (B) time-averaged (10 years) daily water flux and water flux for time-averaged boundary conditions as a function of depth, and (C) standard deviation of water flux as a function of depth (cases 1-4).

Figure 3 Simulated variables with the daily Unsatchem model (M0) for case 4, (A) daily root-zone average TDS with ("R") and without ("NR") chemical reactions, (B) annual drainage salt load *S* with and without reactions, (C) daily root-zone average SAR, (D) daily root-zone average gypsum content.

Figure 4 Daily water balance for the case of shallow water table with net leaching (cases 5-8).

Figure 5 Simulated variables with the daily Unsatchem model (M0) for case 8, (A) daily root-zone average TDS with ("R") and without ("NR") chemical reactions, (B) annual drainage salt load *S* with and without reactions, (C) daily root-zone average SAR, (D) daily root-zone average gypsum content.

Figure 6 Daily water balance for the case of shallow water table without net leaching (cases 9-12).

Figure 7 Simulated variables with the daily Unsatchem model (M0) for case 12, (A) daily root-zone average TDS with ("R") and without ("NR") chemical reactions, (B) annual drainage salt load *S* with and without reactions, (C) daily root-zone average SAR, (D) daily root-zone average gypsum content.

Figure 8 Effect of vertical discretization on predicted average root-zone TDS illustrated for case 4.

Figure 9 Effects of different degrees of heterogeneity, as defined in Table 8, on relative model error.

1

2

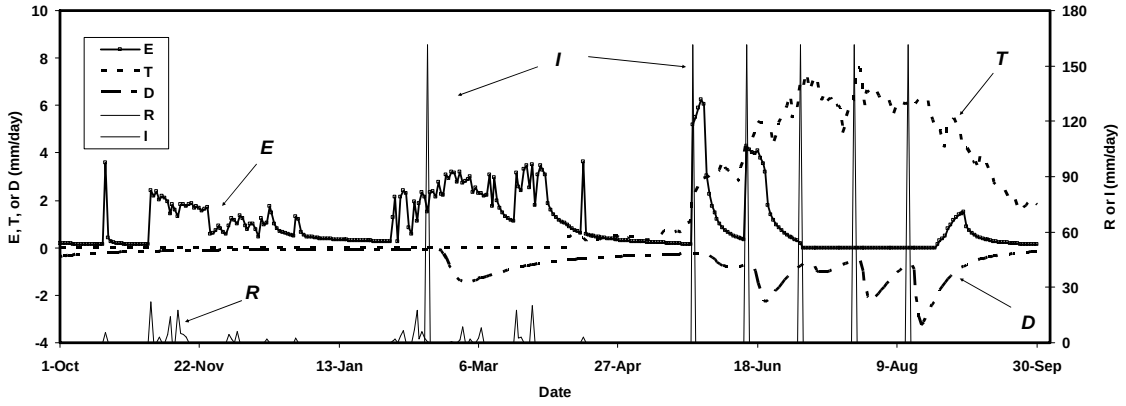

3

4 Figure 1

1

2

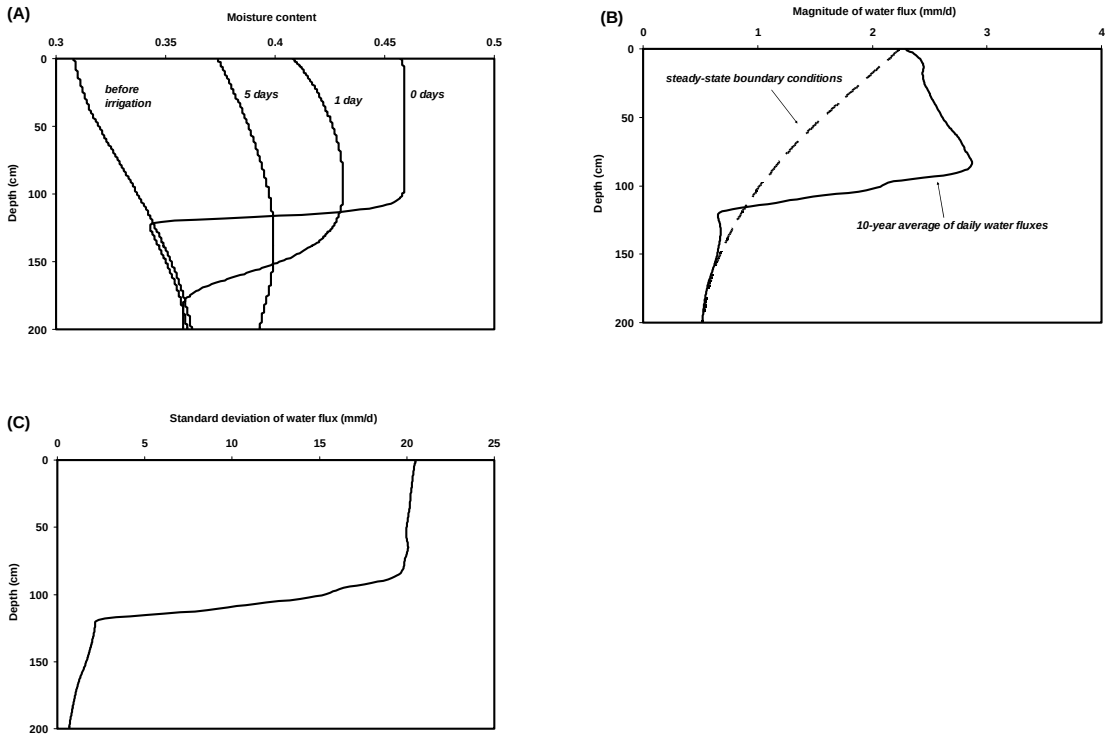

3 Figure 2

4

5

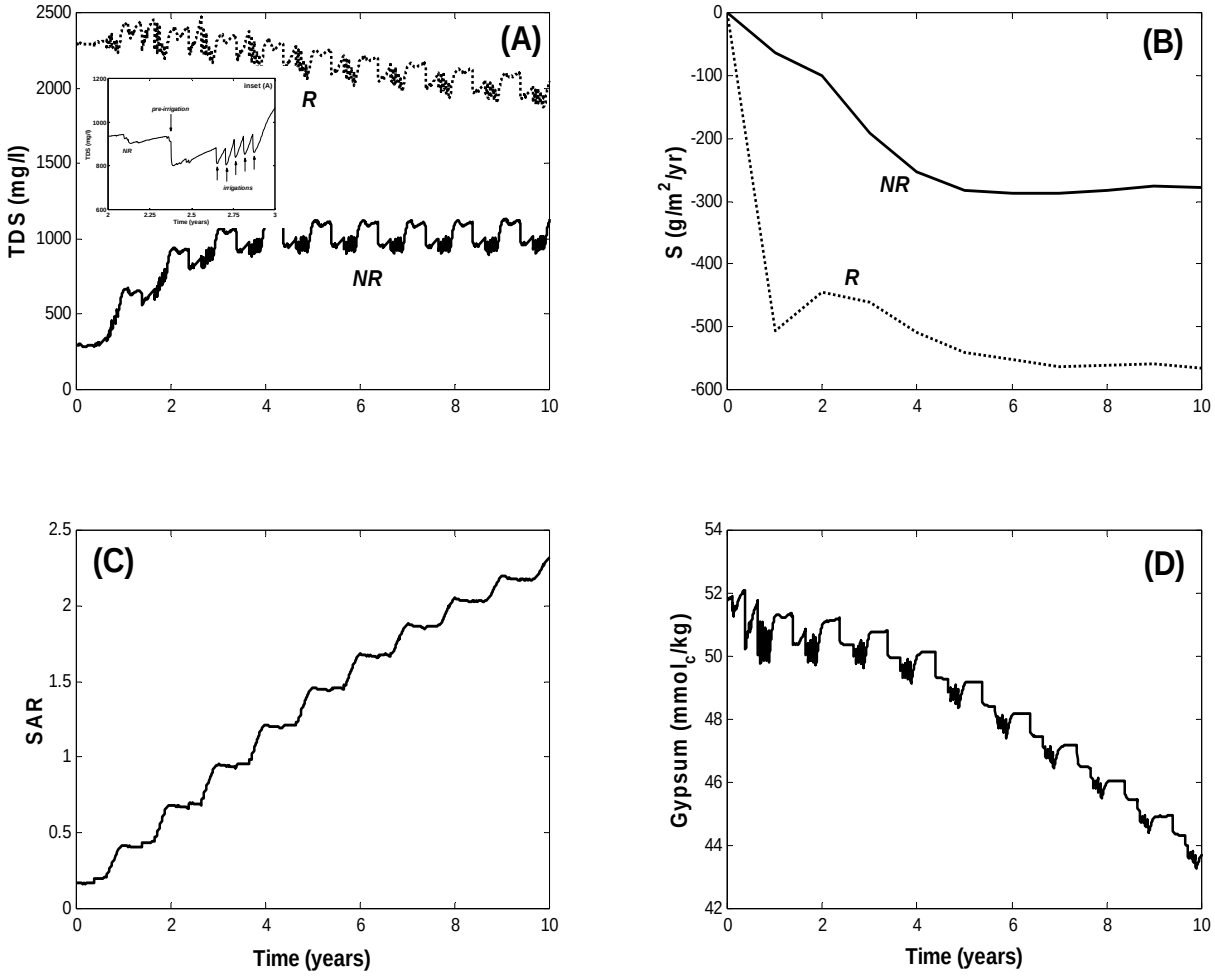
(A)
TDS (mg/l)
R
NR
Inset (A)
pre-irrigation
irrigations
Time (years)
(B)
S (g/m2/yr)
NR
R
(C)
SAR
Time (years)
(D)
Gypsum (mmolc/kg)
Time (years)

1

2 Figure 3

3

1

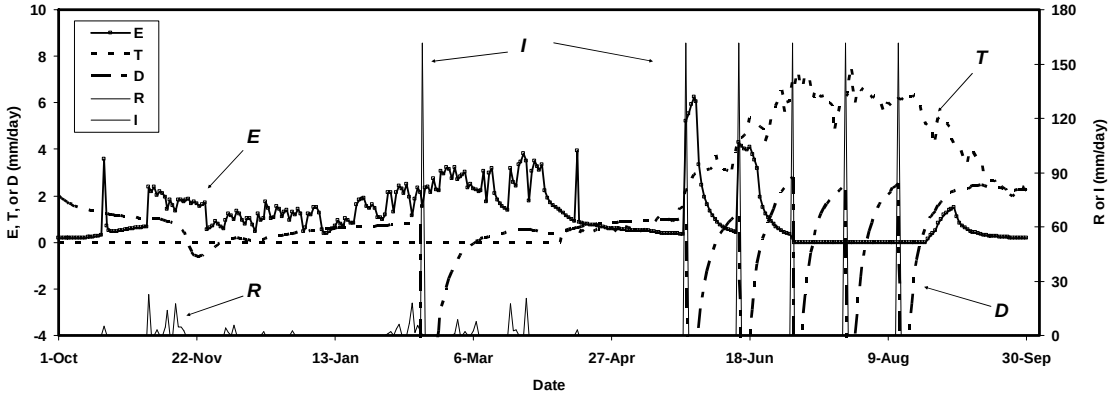
E
T
D
R
I
E
I
T
R
D
E, T, or D (mm/day)
R or I (mm/day)
10
8
6
4
2
0
-2
-4
180
150
120
90
60
30
0
1-Oct
22-Nov
13-Jan
6-Mar
27-Apr
18-Jun
9-Aug
30-Sep
Date

2

3 Figure 4

1

2

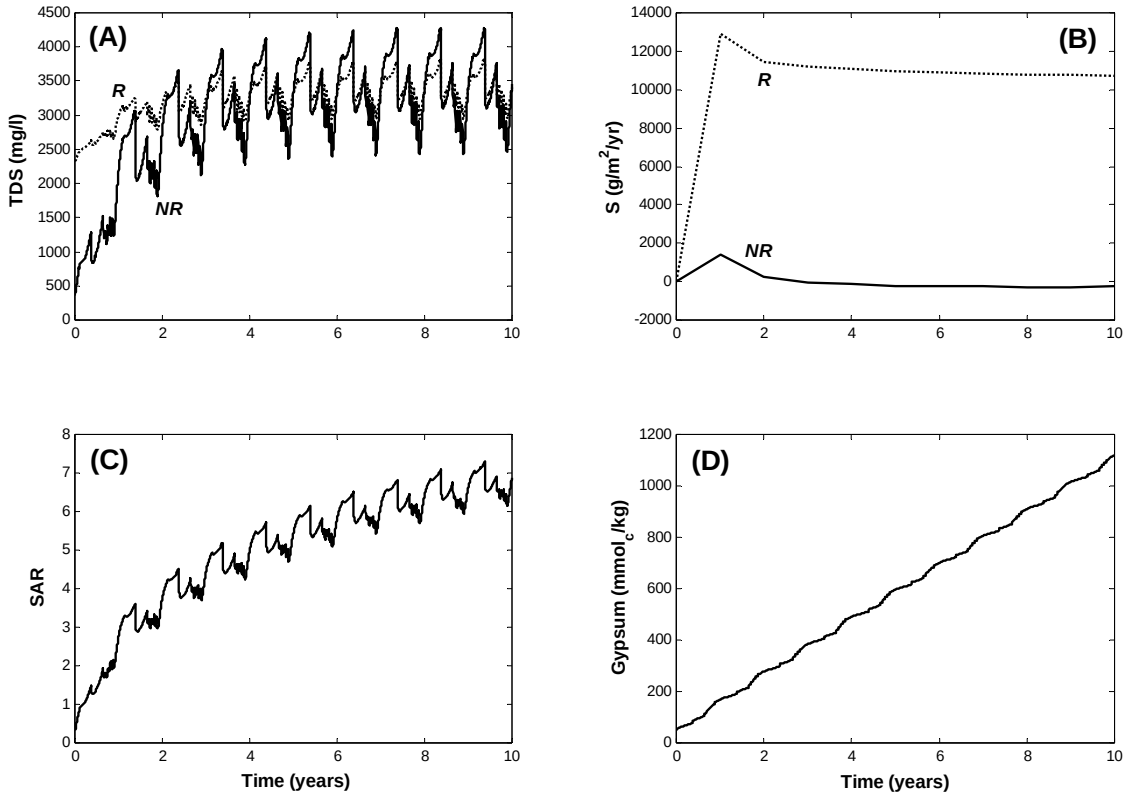

3

4 Figure 5

1

2

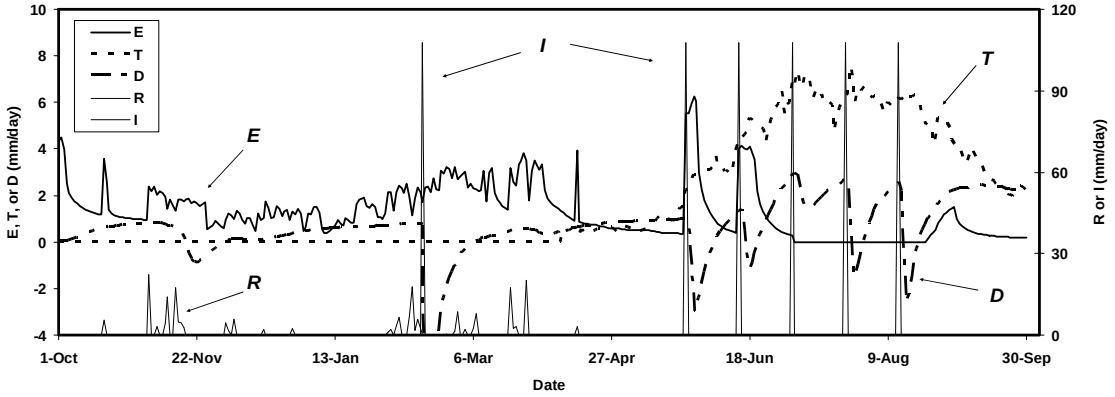

3

4 Figure 6

1

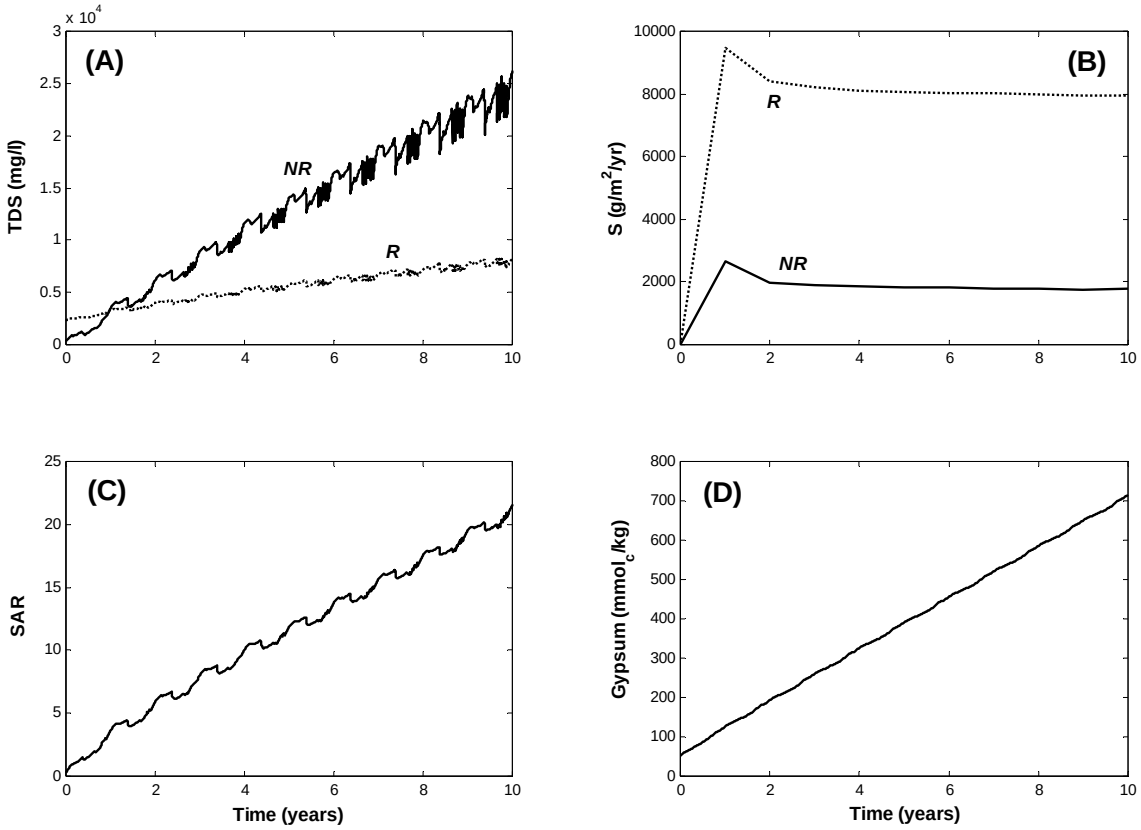

2

3 Figure 7

4

1

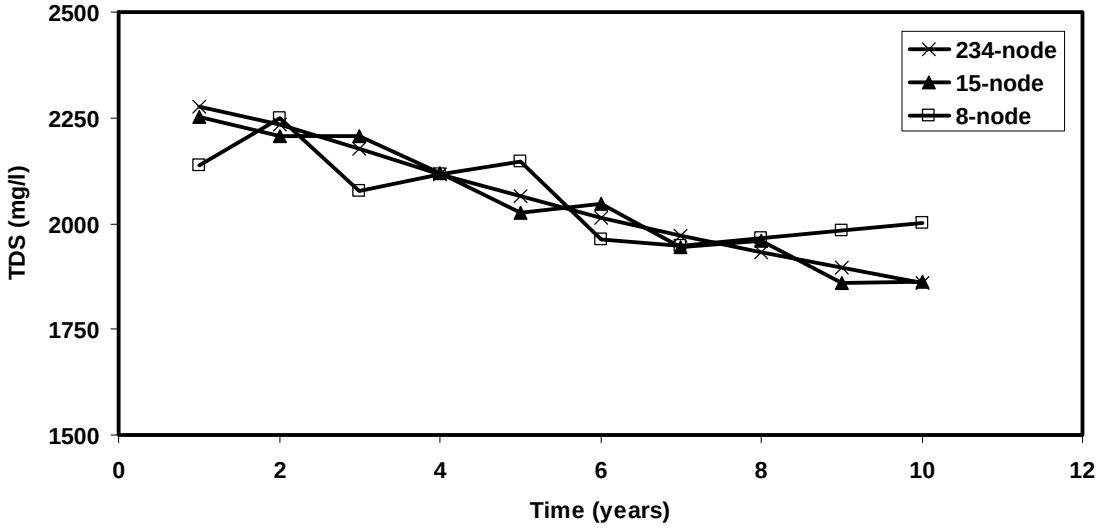

2

3

4 Figure 8

1

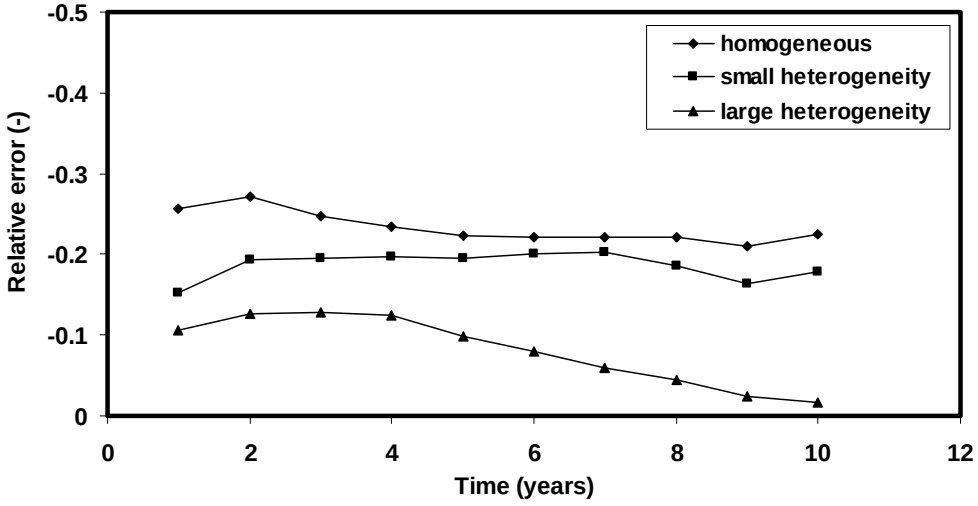

2

3 Figure 9

4